Third International Symposium on Marine Propulsors
smp'13, Launceston, Tasmania, Australia, May 2013

Performance Predictions of a Horizontal Axis Tidal Stream Turbine Considering the Effects of Blade Deformation

Se Wan Park[1], Sunho Park[1], and Shin Hyung Rhee[1,2]

[1]Dept. of Naval Architecture and Ocean Engineering, Seoul National University, Seoul, Korea
[2]Research Institute of Marine Systems Engineering, Seoul National University, Seoul, Korea

ABSTRACT

Flow load induced by tidal stream can cause deformation on the turbine blade of composite material. The deformation adversely affects the turbine performance in many cases. For better designs of tidal stream turbine, analyses considering the effects of blade deformation are necessary. First, the performance prediction of tidal stream turbine were carried out without considering the deformation and in conventional inflow condition, and then its results were compared with existing experimental data. The computed power coefficients for various tip speed ratios (TSR's) were predicted quite closely to the experimental data. Then numerical analyses to consider fluid-structure interaction (FSI) for deformation of the turbine blade were carried out by using partitioned strong coupling method. The blade deformation was clearly observed in the FSI results. The power coefficient, pressure distribution, and detailed flows around the blade were compared between the simulations without and with the deformation.

Keywords

Horizontal Axis Tidal Stream Turbine (HATST), Computational Fluid Dynamics (CFD), Fluid-Structure Interaction (FSI)

1 INTRODUCTION

There are many researches to analyze the performance of horizontal axis tidal stream turbines (HATST) numerically. Lee et al. (2012) developed the blade element momentum theory (BEMT) code and applied to a HATST. The results for the performance prediction of a turbine using BEMT showed similar to that using computational fluid dynamics (CFD) around the design tip speed ratio (TSR) although quite large differences were observed at lower TSR's. Mason-Jones et al. (2008) and Kinnas and Xu (2009) analyzed three-dimensional turbines using CFD. Harrison et al. (2009) and Lee et al/ (2010) studied the wake effect on the turbine performance by using CFD. Besides the general primitive variable-based formulation, McCombes et al. (2009) presented a numerical model based on the vorticity conserving form for unsteady wake modeling of marine current turbines.

Many researches on HATST were done with the assumption that the blade was sufficiently rigid, where the effects of blade deformation were negligible. However, a large chord to span ratio of HATST and high speed tidal current cause deformation of turbine blades. Thus, computations of HATST need to include the fluid-structure interaction (FSI). Nicholls-Lee et al. (2008) optimized tidal energy extraction devices using FSI analysis. They coupled BEM and FEM codes, and developed a FSI simulation procedure for the design of a 20 m diameter 3-bladed HATST.

The present study focused on the numerical analysis of the fluid-structure interaction of a tidal stream energy conversion turbine. In addition, the computational results without and with deformation were compared to each other.

This paper is organized as follows. The description of the physical problem is presented first, and the computational method is followed. Then the computational results are presented and discussed. Finally, concluding remarks are made.

2 NONMENCLATURE

C_P	Power coefficient [-]
C_{press}	Pressure coefficient [-]
R	Radius of turbine [m]
TSR	Tip speed ratio [-]
U□	Free stream velocity [m/s]
ρ	Density [kg/m^3]
Ω	Rotational speed [rad/s]

3 PROBLEM DESCRIPTION

A baseline turbine design was defined to test the feasibility of the developed procedures. A three-bladed HATST with a radius of 4 m was selected. The turbine blade was made of the NACA 63_3-418 foil section, which is popular blade section geometry for wind turbines. The foil shape was used beyond the hub to the blade tip, i.e., between r/R = 0.2 to 1.0. Unlike wind turbines, where a circular shape hub fitting is generally used, a 2:1 elliptic shape was adopted for the hub fitting. Generally, an elliptic hub is stronger than a circular one in flows with less frequent changes of direction such as the one in tidal stream.

The spanwise sections were designed to have various twist angles to extract a uniform lift force from each section. The chord lengths ranged from 0.68 *m* at the root to 0.27 *m* at the blade tip.

The axis of the twist and center of each section were at 0.25*C* and 0.3*C* away from the leading edge, respectively. Here, *C* was the chord length. For the hub fitting part, there was no twist angle and the center was located at 0.5*C*.

The design revolution speed, *Ω*, was 24.72 *rpm*. The operating speed expressed by tip speed ratio (*TSR*) was defined as

$$TSR = \frac{R\Omega}{U_\infty} \tag{1}$$

where U_∞ is the free stream flow. *TSR* was set between 2.7 and 10.4, and the design *TSR* was 5.177. In the present study, *TSR* was varied by changing the free stream flow.

4 COMPUTATIONAL METHODS

4.1 Mathematical Modeling

The equations for the mass and momentum conservations were solved to obtain the velocity and pressure fields, respectively. Once the Reynolds averaging approach for turbulence modeling is applied, the equations for the mass and momentum conservation can be written as

$$\frac{\partial \rho}{\partial t} + \frac{\partial}{\partial x_j}(\rho U_j) = 0 \tag{2}$$

$$\frac{\partial \rho U_i}{\partial t} + \frac{\partial}{\partial x_j}(\rho U_i U_j) = -\frac{\partial p}{\partial x_i} + \frac{\partial}{\partial x_j}(\tau_{ij} - \rho\overline{u_i u_j}) + S_M \tag{3}$$

where *U* is the averaged velocity vector and *p* is the pressure. The unknown term, i.e., the Reynolds stress term, is related to the mean velocity gradients by the Boussinesq hypothesis, as follows:

$$-\rho\overline{u_i u_j} = \mu_t\left(\frac{\partial U_i}{\partial x_j} + \frac{\partial U_j}{\partial x_i}\right) - \frac{2}{3}\delta_{ij}\left(\rho k + \mu_t \frac{\partial U_k}{\partial x_k}\right) \tag{4}$$

where μ_t is the eddy viscosity or turbulent viscosity, which is modeled.

The SST k-ω turbulence model, which is based on the Boussinesq hypothesis with transport equations for the turbulent kinetic energy, *k*, and the turbulent frequency, *ω*, was adopted for turbulence modeling (Menter 1994). The turbulent viscosity is linked to the turbulence kinetic energy and turbulent frequency via the relation:

$$\mu_t = \rho\frac{k}{\omega} \tag{5}$$

The turbulent kinetic energy and the turbulent frequency are obtained from the transport equations, respectively.

$$\frac{\partial(\rho k)}{\partial t} + \frac{\partial}{\partial x_j}(\rho U_j k) = \frac{\partial}{\partial x_j}\left[\left(\mu + \frac{\mu_t}{\sigma_k}\right)\frac{\partial k}{\partial x_j}\right] + P_k - \beta'\rho k\omega + P_{kb} \tag{6}$$

$$\frac{\partial(\rho\omega)}{\partial t} + \frac{\partial}{\partial x_j}(\rho U_j \omega) = \frac{\partial}{\partial x_j}\left[\left(\mu + \frac{\mu_t}{\sigma_\omega}\right)\frac{\partial \omega}{\partial x_j}\right] + a\frac{\omega}{k}P_k - \beta\rho\omega^2 + P_{\omega b} \tag{7}$$

where P_k is the production rate of turbulence, and here the model constants *β'*, *a, β, σ*$_k$, and σ_ω are 0.09, 0.556, 0.075, 2, and 2, respectively. The turbulent viscosity was used to calculate the Reynolds stresses to close the momentum equations. The transport behavior was controlled by a limiter to the formulation of the eddy-viscosity:

$$\nu_t = \frac{a_1 k}{\max(a_1\omega, SF_2)} \tag{8}$$

where

$$\nu_t = \frac{\mu_t}{\rho} \tag{9}$$

F_2 is a blending function, which restricts the limiter to the wall boundary layer, as the underlying assumptions are not correct for free shear flows. *S* is an invariant measure of the strain rate.

4.2 Numerical Methods

A pressure-based finite volume method was employed. Time derivative terms were discretized using the second-order accurate backward implicit scheme, which was generally recommended for most transient computations. The advection terms were discretized using a high resolution scheme, which had second-order accuracy. The velocity-pressure coupling was based on the discretization scheme, proposed by Rhie and Chow (1982). The commercial CFD code, ANSYS CFX 13.0 was used for solving fluid domain. ANSYS Transient Structural was employed for solving the transient structural problem.

4.3 Solution Domain, Boundary Conditions, and Mesh

The Cartesian coordinate system adopted was such that the positive *x*-axis was in the stream-wise direction, the positive *y*-axis toward the right-hand side direction, and the positive *z*-axis was in the vertically upward direction. The origin of the coordinate system was located at the hub center. Thus the *x*-axis was the rotational axis with a rotor revolving in the counter clockwise direction.

A rotating reference frame was used to accommodate the rotation of the rotor in open water conditions. It is one of the simplest approaches for a problem that involves rotating zones. With the rotating reference frame, only one blade needed to be modeled with periodic boundaries on the sides. The computational domain extent was a length of *9D* and a radius of *3D*, where *D* represented the turbine diameter. The inlet and outlet boundaries were located at *3D* upstream and *6D* downstream, respectively.

Figure 1 shows the boundary conditions and domain extent designed for the pre sent computation. The Dirichlet boundary condition, i.e., the specified value of the velocity, was applied on the inlet boundary. On the exit boundary, the reference pressure with extrapolated velocity was applied. The free slip wall boundary condition was applied on the far-field boundary. A no-slip condition and FSI interface condition was applied on

the turbine blade surfaces. Non-matching interfaces, between the sub-domain encompassing the turbine blade and outer sub-domains, were defined and solved using the general grid interface (GGI) interpolation method. On the side boundary, to take the rotational flow into account, the flow across the two opposite planes was assumed to be identical, i.e., periodic.

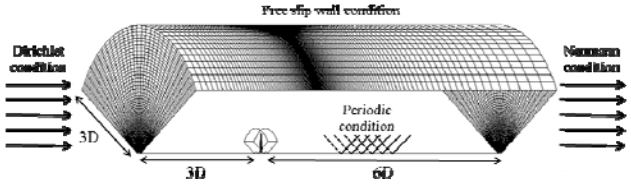

Figure 1 Computational domain for the CFD analysis

To develop a convenient procedure for performance prediction, hybrid meshing was used (Lee et al., 2012). The whole domain was divided into several sub-domains, and among the sub-domains, the one with the blade was filled with tetrahedral cells and the others with simple geometry were filled with hexahedral cells for high quality solution, as shown in Figure 2. By this approach, it was possible to get rid of the difficulty of mesh generation around complex geometry.

On the rotating turbine blade, a high speed flow occurs near the blade tip and low pressure appears near the leading edge and at the blade tip on the suction side. Accurate prediction of the low pressure on the suction side is necessary for the high fidelity performance prediction of turbines. Thus, the blade surface near the leading edge, trailing edge, and blade tip were filled with finer cells. An unstructured mesh consisting of 2 million cells in the domain were generated and employed for the computations.

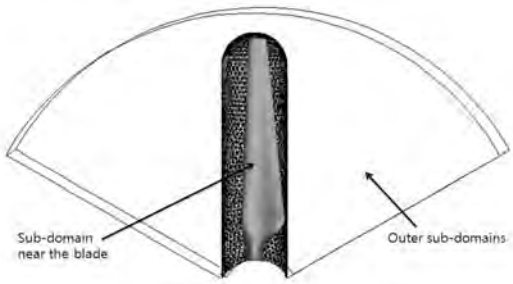

Figure 2 Sub-domain near the blade for the CFD analysis

Figure 3 shows the surface mesh for the finite element analysis. For more accurate prediction of deformation, fine meshes were distributed near the leading edge of the blade. The structured surface mesh consisted of 70 cells in the chord-wise and 15 cells in the span-wise directions. The turbine blade is constructed of E-glass reinforcing fiber, and its material property is shown in Table 1 (Shenoi and Wellicome, 1993).

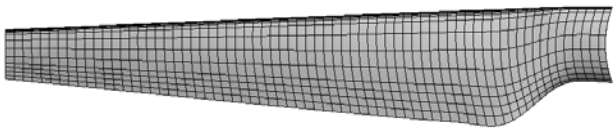

Figure 3 Surface meshes for the structural analysis

Table 1 Mechanical properties of the unidirectional E-glass/epoxy composite (Daniel and Ishai, 1994)

Property	Value
$\rho\ (kg/m^3)$	2100
$E_1\,(GPa)$	39
$E_2\,(GPa)$	8.6
$G_{12}\,(GPa)$	3.8
υ_{12}	0.28

4.4 Verification Test

To verify the developed CFD procedure, the results from the model scale experiment reported by Bahaj et al. (2007) were used. A three-bladed 800 *mm* diameter turbine was used. The blade geometry was defined with 17 sections in the span-wise direction. Each blade section took the profile shape of a NACA 63-8xx. The chord, thickness, and pitch distribution were also provided. A commercial CAD tool, CATIA, was used to construct the blade geometry with the given information. Figure 4 shows the test rig in the cavitation tunnel and the CAD constructed blade geometry.

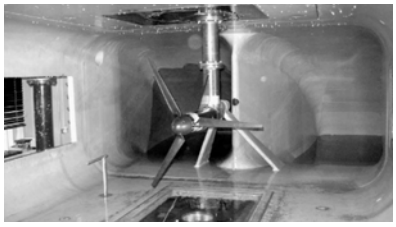

Fig. 4 Photograph of the test rig (Bahaj et al. 2007)

The experiments were done in a 2.4 m × 1.2 m cavitation tunnel. The results for the power coefficient were presented for a wide range of *TSR*. The turbine performance was analyzed for a 0^o yaw angle and 25^o hub pitch angle conditions. The turbine dimensions and inflow velocity of 1.54 *m/s* were the same for both the measurements and CFD predictions. Note that the hub, however, was not considered in the CFD simulations. Only one blade was used for the prediction since a rotating reference frame method was employed. Figure 5 shows the power coefficient ($C_P = P/0.5\rho A U_\infty^3$) over a range of *TSR* measured by the experiment and predicted by the present CFD method. The present CFD results agree well with the experimental data, confirming that the developed procedure predicts the turbine performance quite well.

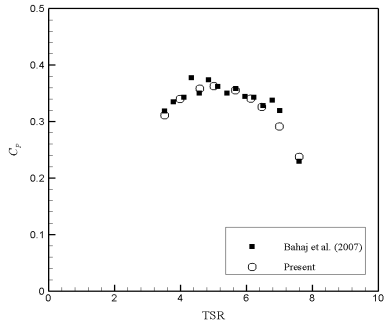

Figure 5 Verification for the C_P

5 RESULTS AND DISCUSSION

Before FSI analysis, the computation of the flow around the baseline turbine without considering the deformation was performed using the verified computational methods. Figure 6 shows the predicted C_P over a range of various *TSR*s, presenting a typical trend of the power performance curve for a three-bladed tidal turbine. The peak power coefficient was predicted at the design *TSR*, 5.2.

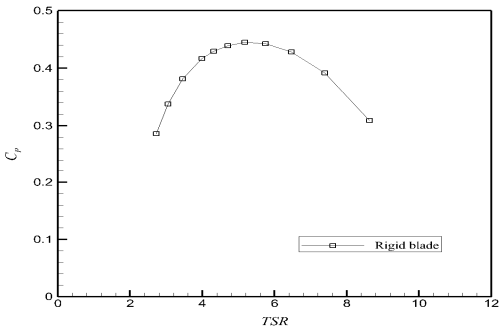

Figure 6 C_P curve of the baseline turbine

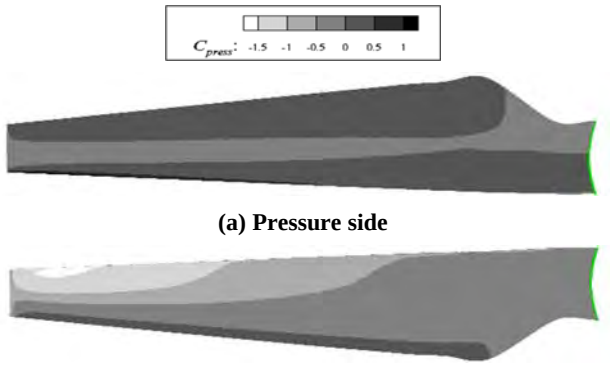

(a) Pressure side

(b) Suction side

Figure 7 Surface C_{press} contours on the pressure and suction sides by the simulation w/o the blade deformation

Figure 7 shows the surface pressure coefficient (C_{press} = $(P_L-P_O)/0.5\rho U_\infty^2$) contours on the pressure and suction sides of the baseline turbine at the design *TSR*. The lowest pressure was seen at the leading edge on the suction side near the blade tip. Meanwhile, the highest pressure was observed at the leading edge on the pressure side. The pressure difference between the two sides generates the lift force on the blade, and thereby the torque on the turbine. From the pressure coefficient contours, it was obvious that most of the power was produced near the blade tip.

The FSI analysis was carried out at the design *TSR*. The tidal current caused deformation of the blade, and the deformation reached an equilibrium level, at which the fluid force and structure restoring force were balanced. Figure 8 shows the tip displacement of the baseline turbine blade. The predicted equivalent displacement at the blade tip was 0.118 *m*. Figure 9 shows the deformed shape of the blade in true scale. The turbine blade was bent toward the downstream. Figure 10 shows the von Mises stress distribution on the pressure and suction sides of the blade. The maximum stress was observed at the mid-chord for the range of *r/R*=0.4~0.5.

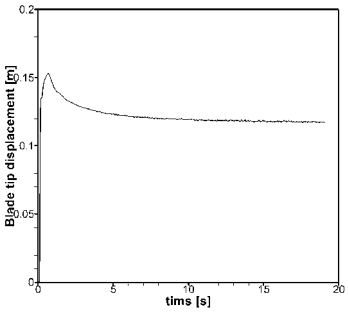

Figure 8 Blade tip displacement

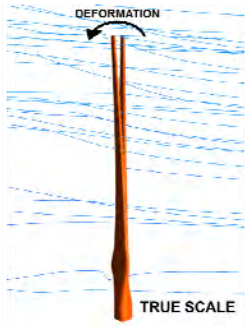

Figure 9 Deformed blade shape

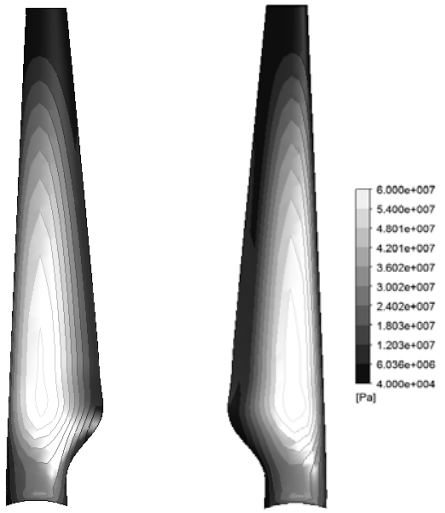

(a) Pressure side **(b) Suction side**

Figure 10 von Mises Stress distribution

Figure 11 shows the surface pressure coefficient contours on the pressure and suction sides of the baseline turbine including the deformation at the design *TSR*. The lowest pressure was also seen at the leading edge on the suction side near the blade tip. The pressure coefficient on the suction side was overall lower than that without considering the deformation. The blade deformation reduced the pressure drop at the suction side. Therefore, the computation without considering the deformation could over-predict the cavitation, if estimated by the minimum pressure on the suction side.

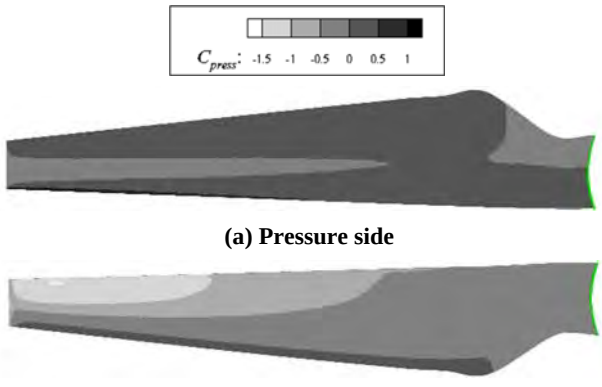

(a) Pressure side

(b) Suction side

Figure 11 Surface C_{press} contours on the pressure and suction sides by the simulation w/ the blade deformation

Fig. 12 shows the power coefficient predicted for the cases without and with the deformation. In the case of the deformation considered, the power coefficient was 1.7% lower at the design *TSR*. Namely, the computation without considering the deformation could over-predict the turbine performance.

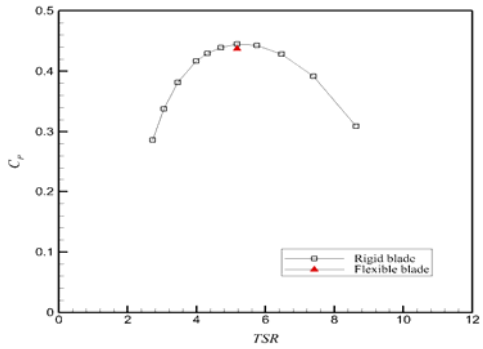

Fig. 12 Comparison of the C_P by the simulations w/o and w/ the deformation

Figure 13 shows the vorticity magnitude contours at the downstream of the blade. The predicted maximum vorticity level was lower by considering the deformation. As shown in Figure 13, maximum vorticity level was reduced and narrowed for flexible blade, 22.27% lower of maximum vorticity magnitude than rigid blade. In other words, the simulation with a rigid blade could over-estimate the noise and vibration problem of the turbine, which confirms that the FSI analysis is essential in predicting the performance of a HATST more accurately.

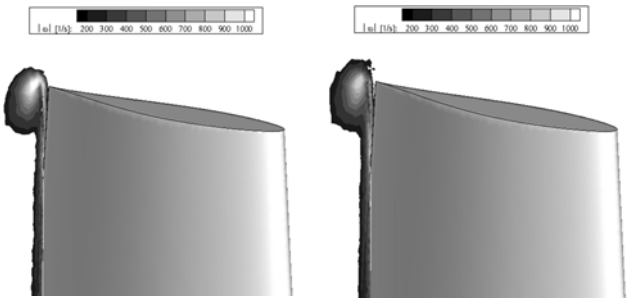

(a) Rigid blade **(b) Flexible blade**

Figure 13 Vorticity magnitude contours

6 CONCLUSIONS

The FSI analysis was performed for a HATST. The computational method for performance prediction of a turbine was verified by comparison against existing experimental data. The power coefficients over a range of *TSR* showed good agreement.

CFD analysis without considering the deformation was done for TSR's between 2.7 and 10.4. And the FSI analysis was performed at the design TSR. In the FSI analysis, the deformation of the blade tip was predicted. It is suggested that FSI analysis should be considered for better turbine blade design.

ACKNOWLEDGMENTS

This work was supported by World Class University Project (R32-2008-000-10161-0) and Multi-Phenomena CFD Research Center (20090093103) funded by the Ministry of Education, Science and Technology of the Korea government, and by the Agency for Defense Development (411115-911013101-712).

REFERENCES

Bahaj, A.S., Molland, A.F., Chaplin, J.R., Batten W.M.J. (2007). 'Power and thrust measurements of marine current turbines under various hydrodynamic flow conditions in a cavitation tunnel and a towing tank', Renewable Energy **32**, pp.407-426.

Harrison, M.E., Batten, W.M.J., Myers, L.E., Bahaj, A.S. (2010). 'A comparison between CFD simulations and experiments for predicting the far wake of horizontal axis tidal turbines', IET Renewable Power Generation **4**(6), pp. 613-617

Kinnas, S.A., Xu, W. (2009). 'Analysis of tidal turbines with various numerical methods', 1st Annual MREC Technical Conference, MA, USA

Lee, J. H., Park S., Kim, D. H., Rhee, S. H., Kim, M. C. (2012). 'Computational methods for performance analysis of horizontal axis tidal stream turbines', Applied Energy **98**, pp.512-523.

Lee, S.H., Lee, S.H., Jang, K., Lee, J., Hur, N. (2010). 'A numerical study for the optimal arrangement of ocean current turbine generators in the ocean current power parks', Current Applied Physics **10**, pp.137–141.

McCombes, T., Johnstone, C., Grant, A. (2009). 'Unsteady 3D wake modeling for marine current turbines', 8th European Wave and Tidal Energy Conference, Uppsala, Sweden

Mason-Jones, A., O'Doherty, T., O'Doherty, D.M., Evans, P.S., Wooldridge, C.F. (2008). 'Characterisation of a HATT using CFD and ADCP site data', 10th World Renewable Energy Congress, Grasgow.

Menter, F.R. (1994). 'Two-equation eddy-viscosity turbulence models for engineering applications', AIAA-Journal. **32**(8), pp.1598-1605.

Nicholls-Lee, R.F., Turnock, S.R., and Boyd, S.W. (2008). 'Simulation based optimization of marine current turbine blades', 7th International Conference on Computer and IT Applications in the Maritime Industries, Liege, Belgium

Nicholls-Lee, R.F., Turnock, S.R., and Boyd, S.W. (2011). 'A method for analysing fluid structure interactions on a horizontal axis tidal turbine', 9th European Wave and Tidal Energy Conference, Southampton, UK

Rhie, C.M. and Chow, W.L. (1982). 'A numerical study of the turbulent flow past an isolated airfoil with trailing edge separation', AIAA Paper 82-0998.

Danel I.M. and Ishai O. (1994). Engineering Mechanics of Composite Materials, OXFORD UNIVERSITY PRESS